Engineering Journal issn: 0125-8281

Article

Structural Analysis of Mini Power Weeder Worm and Worm Gear with Three Different Materials

Zaw Htet Win[a], War War Min Swe[b,*], and Aung Ko Latt[c,*]

Mechanical Engineering Department, Mandalay Technological University, Myanmar
E-mail: [a]zawhtetwin1991@gmail.com, [b,*]warwarminswe288@gmail.com (corresponding author), [c,*]dr.aungkolat@gmail.com (corresponding author)

Abstract. The main aim of this paper is to conduct the structural analysis of min power weeder worm and worm gear with three different materials. The objectives of this paper are to calculate the design of worm and worm gear, to draw the model of worm and worm gear by using AutoCAD 2019 software, to analyze the structural behavior of worm and worm gear by theoretical approach using von-Mises criteria and compare with numerical structural result using ANSYS 16.2 software, and to select the suitable material of worm and worm gear for good performance. A 2.5 hp engine power and 6000 rpm worm speed mini power weeder is used in this paper to do worm and worm gear bending stress analysis with material properties of phosphor bronze, aluminum bronze, and tin bronze material. For the phosphor bronze material, the lowest von-Mises stress and effective strain are obtained. Thus, phosphor bronze is found to be the suitable material for worm and worm gear.

Keywords: Mini power weeder, worm and worm gear, static structural analysis, von-Mises Stress, phosphor bronze.

ENGINEERING JOURNAL Volume 28 Issue 3
Received 23 November 2023
Accepted 21 March 2024
Published 31 March 2024
Online at https://engj.org/
DOI:10.4186/ej.2024.28.3.35

DOI:10.4186/ej.2024.28.3.35

1. Introduction

Agriculture is the main industry in Myanmar. In modern days, industry farming is a way to make easier for their workplace than before. As a result, farm machinery has been progressed in many places of the world. Within many agricultural use, mini power weeder is useful for even those people who use for home gardening because this is very easy and comfortable [1].

The main parts of mini power weeder are drive shaft, worm and worm gear, and weeder blade [2]. In mini power weeder, the drive shaft forms a direct link between the engine and gear drive assembly. Worm and worm gear design play an important role for transmission system in mini power weeder. Worm gear consists of worm and worm wheel [3]. Blades are the main part of mini power weeder which are directly engaged with the soil for harvesting the weed from root and loosening of upper layer soil.

The real problem for this research is gear failure. There are important things about gear failure are moderate wear and tear, excessive wear and tear, abrasive damage, corrosion, frosting, spalling, pitting, and breakage [4]. Bronze is often most desirable because it offers a winning combination of high strength-to-weight ratio, high resistance to wear, the ability to enhance the physical properties through heat treatment, and competitive pricing [5].

In 2016, Engr. Rufus O. Chime presented static structural analysis of worm gear by using CAD (Computer-Aided-Design) simulation [6]. In 2018, May Phyoe Thu studied contact stress analysis of stainless steel spur gear by theoretical method using Hertz equation and Finite element analysis using ANSYS 16.0 Workbench [7]. Figure 1 shows the assembly of worm and worm gear in mini power weeder. The specification data for worm and worm gear of mini power weeder are obtained from "Farm Machinery Factory, Mandalay Industrial Zone".

Fig. 1. Assembly of worm and worm gear [8].

2. Methodology

There are three steps to solve the machinery breakdown because of the gear failure. The first step is design and stress calculation of worm and worm gear by theoretically. The second step is modelling the worm and worm gear with AutoCAD 2019 software. The third step is static structural analysis with ANSYS 16.2 software.

2.1. Design Consideration of Worm and Worm Gear

In designing worm and worm gear, the quantities like engine power, worm speed, face length of worm, and center distance between the shafts are used as specification data which is shown in Table 1.

Table 1. Specification data for worm and worm gear.

Parameters	Symbol	Value	Unit
Engine power	P	2.5	hp
Worm speed	N_w	6000	rpm
Face length of worm	L_w	58	mm
Center distance	C	40	mm

The pitch circle diameter of worm,

$$D_w = \frac{C^{0.875}}{1.416} = 3P_c \quad (1)$$

The circular pitch of worm gear,

$$P_c = \pi m_a \quad (2)$$

Axial module,

$$m_a = \frac{D_w}{3\pi} \quad (3)$$

Pitch circle diameter of worm gear,

$$D_g = m_a n_g \quad (4)$$

Actual pitch circle diameter of worm,

$$D_w = 2C - D_g \quad (5)$$

Axial pitch of worm,

$$P_a = \pi m_a \quad (6)$$

The lead,

$$L = P_a n \quad (7)$$

Lead angle,

$$\lambda = tan^{-1}\left(\frac{L}{\pi D_w}\right) \quad (8)$$

Face width of worm gear,

$$b = 2.38P_a + 6.5 \quad (9)$$

Rubbing speed,

$$V_r = \frac{\pi D_w N_w}{cos\lambda} \quad (10)$$

The coefficient of friction,

$$\mu = 0.025 + \frac{V_r}{18000} \quad (11)$$

Angle of friction,

$$\phi_1 = tan^{-1}\mu \quad (12)$$

Efficiency of worm gearing,

$$\eta = \frac{tan\lambda}{tan(\lambda+\phi_1)} \quad (13)$$

Table 2. Result data for worm and worm gear.

Parameters	Symbol	Value	Unit
Axial module	m_a	2	mm
Pitch circle diameter of worm gear	D_g	58	mm
Pitch circle diameter of worm	D_w	22	mm
Axial pitch of worm	P_a	6.283	mm
Lead of worm	L	6.283	mm
Lead angle	λ	5.194	deg
Face width of worm gear	b	21.454	mm
Efficiency of worm gearing	η	65.092	%

2.2. Proportions Consideration of Worm and Worm Gear

The various proportions for worm and worm gear in term of the axial or circular pitch in (mm) are shown in Table 3.

Table 3. Proportions for worm and worm gear.

Parameters	Symbol	Single and double threaded
Addendum	a	$0.318P_c$
Dedendum	d	$0.368P_c$
Tooth depth	h	$0.686P_c$
Root diameter of worm	D_{rw}	$D_w - 2D$
Outside diameter of worm	D_{ow}	$D_w + 2a$
Root diameter of worm gear	D_{rg}	$D_g - 0.736P_c$
Outside diameter of worm gear	D_{og}	$D_g + 1.0135P_c$
Throat diameter of worm gear	D_t	$D_g + 0.636P_c$
Radius of gear face	R_f	$0.822P_c + 14$
Radius of gear rim	R_r	$2.2P_c + 14$

The worm and worm gear in mesh is shown in Fig. 2.

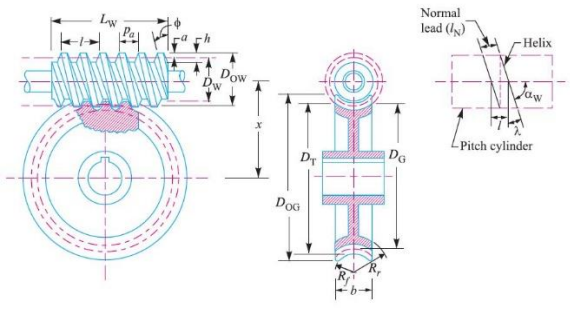

Fig. 2. Worm and worm gear.

Table 4. Result data for worm and worm gear proportions.

Parameters	Symbol	Value	Unit
Addendum	a	1.998	mm
Dedendum	d	2.312	mm
Tooth depth	h	4.310	mm
Root diameter of worm	D_{rw}	17.376	mm
Outside diameter of worm	D_{ow}	25.996	mm
Root diameter of worm gear	D_{rg}	53.376	mm
Outside diameter of worm gear	D_{og}	64.368	mm
Throat diameter of worm gear	D_t	61.996	mm
Radius of gear face	R_f	19.165	mm
Radius of gear rim	R_r	27.823	mm

2.3. Strength and Dynamic Check of Worm and Worm Gear

For strength check,

Transmitted torque on worm,

$$T_w = \frac{P \times 60}{2\pi N_w} \quad (14)$$

Actual transmitted tooth load,

$$F_t = \frac{2T_w}{D_w} \quad (15)$$

In the strength check of worm gear tooth, permissible tangential tooth load is calculated by using Eq. (16).

$$F_T = \sigma_0 C_v b \pi y m_a \quad (16)$$

where σ_0 = allowable static stress;
C_v = velocity factor;
y = Lewis form factor.

Allowable static stress σ_0 is 84 MPa for phosphor bronze material [9].

Velocity factor,

$$C_v = \frac{6}{6+V_g} \quad (17)$$

where V_g = peripheral velocity of worm gear.

Peripheral velocity of worm gear,

$$V_g = \frac{\pi D_g N_g}{60} \quad (18)$$

The tooth form factor,

$$y = 0.124 - \frac{0.684}{n_g} \quad (19)$$

The actual transmitted tooth load is less than the permissible tangential tooth load, so the design is satisfying.

For dynamics check,

The dynamics tooth load,

$$F_d = \frac{F_t}{C_v} \quad (20)$$

The static tooth load,

$$F_s = \sigma_e b \pi y m_a \quad (21)$$

where σ_e = flexural endurance limit.

Flexural endurance limit σ_e is 168 MPa for phosphor bronze material.

The wear tooth load,

$$F_w = D_g b K \quad (22)$$

where K = load stress factor.

Load stress factor K is 0.55 MPa for phosphor bronze material [10].

The dynamics tooth load is less than static tooth load and wear tooth load, so the design is satisfying.

Strength and dynamic check are essential for design of worm and worm gear calculation to work properly in the machine. Worm and worm gear will damage easily and will not be able to perform with fully load when strength and dynamic check did not consider when design calculation was done [11]. Therefore, five tooth loads are calculated for strength and dynamic check. For the strength check, the actual transmitted tooth load must be less than permissible tangential tooth load. For the dynamic check, the static tooth load and wear tooth load must be greater than dynamics tooth load [12]. These tooth load results are shown in Table 5.

Table 5. Result data for strength and dynamic check.

Parameters	Symbol	Value	Unit
Actual transmitted tooth load	F_t	269.731	N
Permissible tangential tooth load	F_T	1024.745	N
Dynamics tooth load	F_d	298.045	N
Static tooth load	F_s	2264.631	N
Wear tooth load	F_w	684.383	N

Figure 3 shows the forces acting on the worm. The forces on a worm gear are equal in magnitude to that of worm, but opposite in direction [13] as shown in Fig. 3.

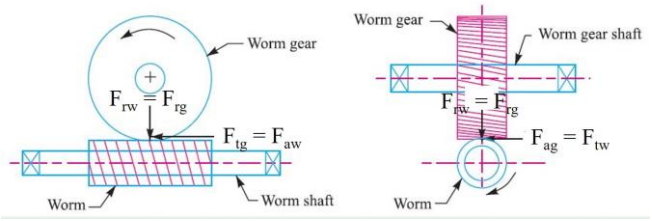

Fig. 3. Forces acting on worm teeth.

Torque acting on worm gear,

$$T_g = T_w V R \eta \quad (23)$$

The tangential force on the worm is equal to the axial force on the worm gear is calculated by using Eq. (24).

$$F_{tw} = F_{ag} = \frac{2T_w}{D_w} \quad (24)$$

The axial force acting on worm is equal to the tangential force on the worm gear is calculated by using Eq. (25).

$$F_{aw} = F_{tg} = \frac{2T_g}{D_g} \quad (25)$$

The radial force of worm and worm gear is calculated by using Eq. (26).

$$F_{rw} = F_{rg} = F_{aw} \tan \phi \quad (26)$$

Each torque is acting on worm and worm gear as transmitted torque because of the rotation of worm and worm gear. Therefore, a contact point between the surface of worm and worm gear is affected by axial, tangential, and radial forces together [14]. At this point, tangential force on worm and axial force on worm gear are equal because tangential force is perpendicular to the axis of rotation. Axial force on worm and tangential force on worm gear are equal because axial force is parallel to the axis of rotation. Radial forces on worm and worm gear are equal because radial force is always applied from the center of worm and worm gear towards the contact point [15]. Result of each torque and forces acting on worm and worm gear are shown in Table 6.

Table 6. Result data for forces acting on worm and worm gear.

Parameters	Symbol	Value	Unit
Torque acting on worm	T_w	2.967	Nm
Torque acting on worm gear	T_g	56.007	Nm
Tangential force on worm	F_{tw}	269.727	N
Axial force on worm	F_{aw}	1931.276	N
Radial force on worm	F_{rw}	499.462	N
Tangential force on worm gear	F_{tg}	1931.276	N
Axial force on worm gear	F_{ag}	269.727	N
Radial force on worm gear	F_{rg}	499.462	N

2.4. Design Calculation of Worm Shaft

Torque on the worm gear shaft,

$$T_{gs} = \frac{1.25 \times P \times 60}{2\pi n_g} \quad (27)$$

Torque acting on the worm shaft,

$$T_{ws} = \frac{T_{gs}}{\eta \times V R} \quad (28)$$

Tangential force on the worm shaft,

$$F_{ts} = \frac{2T_{ws}}{D_w} \quad (29)$$

Axial force on the worm shaft,

$$F_{as} = \frac{2T_{gs}}{D_g} \quad (30)$$

Radial force on the worm shaft,

$$F_{rs} = F_{as} \tan \phi \quad (31)$$

Bending moment due to radial force,

$$BM_R = \frac{F_{rs} \times D_g}{4} \quad (32)$$

Bending moment due to axial force,

$$BM_A = \frac{F_{as} \times D_w}{4} \quad (33)$$

Total bending moment in the vertical plane,

$$M_V = BM_A + BM_R \quad (34)$$

Bending moment in the horizontal plane,

$$M_H = BM_T = \frac{F_{ts} \times D_g}{4} \quad (35)$$

Resultant bending moment on the worm shaft,

$$M_W = \sqrt{M_H^2 + M_V^2} \quad (36)$$

The equivalent twisting moment on the worm shaft,

$$T_{ew} = \sqrt{T_{ws}^2 + M_W^2} \quad (37)$$

Diameter of the worm shaft,

$$d_w^3 = \frac{16 T_{ew}}{\pi \tau} \quad (38)$$

Table 7. Result data for worm shaft.

Parameters	Symbol	Value	Unit
Torque on the worm gear shaft	T_{gs}	107.555	Nm
Torque acting on the worm shaft	T_{ws}	5.698	Nm
Tangential force on the worm shaft	F_{ts}	518	N
Axial force on the worm shaft	F_{as}	3708.793	N
Radial force on the worm shaft	F_{rs}	959.159	N
Bending moment due to radial force	BM_R	13.908	Nm
Bending moment due to axial force	BM_A	20.398	Nm
Total bending moment in the vertical plane	M_V	34.306	Nm
Bending moment in the horizontal plane	M_H	7.511	Nm
Resultant bending moment on the worm shaft	M_W	35.119	Nm
The equivalent twisting moment on the worm shaft	T_{ew}	35.578	Nm
Diameter of the worm shaft	d_w	12	mm

2.5. Design Calculation of Bearing Selection

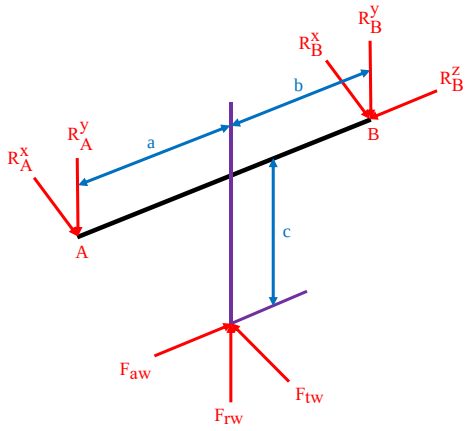

Fig. 4. Forces applied to worm shaft [16, 17].

Considering the equilibrium of axial forces,

$$F_{aw} = R_B^z \quad (39)$$

Taking moment of forces in the Y axis about A,

$$R_B^x \times (a+b) - F_{tw} \times (a) = 0 \quad (40)$$

Summation of forces in the X axis about zero,

$$\sum F_x = 0$$

$$R_A^x + R_B^x - F_{tw} = 0 \quad (41)$$

Taking moment of forces in the X axis about A,

$$R_B^y \times (a+b) - F_{rw} \times (a) - F_{aw} \times (c) = 0 \quad (42)$$

Summation of forces in the Y axis about zero,

$$\sum F_y = 0$$

$$R_A^y + R_B^y - F_{rw} = 0 \quad (43)$$

For bearing A,

Radial load at A,

$$F_r = \sqrt{(R_A^x)^2 + (R_A^y)^2} \quad (44)$$

For bearing B,

Radial load at B,

$$F_r = \sqrt{(R_B^x)^2 + (R_B^y)^2} \quad (45)$$

Equivalent bearing load,

$$P = XVF_r \quad (46)$$

Life of bearing in million revolution,

$$L_{rev} = \frac{60 N L_h}{10^6} \quad (47)$$

Basic dynamic load,

$$C = P \times \sqrt[3]{L_{rev}} \quad (48)$$

DOI:10.4186/ej.2024.28.3.35

Table 8. Result data for bearing A.

Parameters	Symbol	Value	Unit
Horizontal reaction force at A	R_A^x	147.351	N
Vertical reaction force at A	R_A^y	76.150	N
Radial load at A	F_r	165.865	N
Equivalent bearing load	P	165.865	N
Life of bearing in million revolution	L_{rev}	2160	-
Basic dynamic load	C	2.144	kN
Inner diameter	d	12	mm
Outer diameter	D	24	mm
Face width	B	6	mm

Select the bearing number 6901 single-row deep groove ball bearing for bearing A.

Table 9. Result data for bearing B.

Parameters	Symbol	Value	Unit
Horizontal reaction force at B	R_B^x	122.376	N
Vertical reaction force at B	R_B^y	423.312	N
Radial load at B	F_r	440.646	N
Equivalent bearing load	P	440.646	N
Life of bearing in million revolution	L_{rev}	2160	-
Basic dynamic load	C	5.696	kN
Inner diameter	d	12	mm
Outer diameter	D	32	mm
Face width	B	10	mm

Select the bearing number 6201 single-row deep groove ball bearing for bearing B.

2.6. Calculation of Shear Force and Bending Moment of Worm Shaft

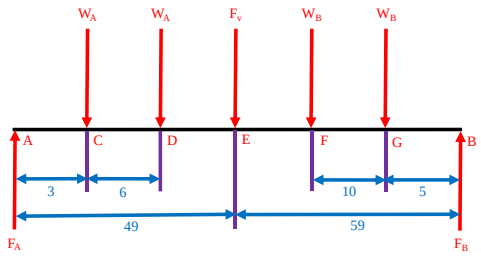

Fig. 5. Force diagram of worm shaft [18].

$$\sum F_y = 0$$
$$F_A - 2W_A - F_v - 2W_B + F_B = 0 \quad (49)$$
$$\sum M_A = 0$$
$$12W_A + 196W_B + 49F_v - 108F_B = 0 \quad (50)$$

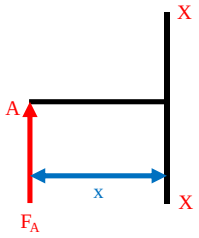

Fig. 6. Span AC (0 < x < 3).

$$SF_{XX} = F_A \quad (51)$$
$$BM_{XX} = F_A \times (x) \quad (52)$$

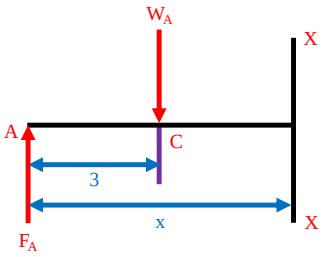

Fig. 7. Span CD (3 < x < 9).

$$SF_{XX} = F_A - W_A \quad (53)$$
$$BM_{XX} = F_A \times (x) - W_A \times (x-3) \quad (54)$$

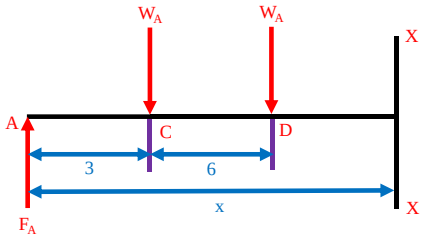

Fig. 8. Span DE (9 < x < 49).

$$SF_{XX} = F_A - 2W_A \quad (55)$$
$$BM_{XX} = F_A \times (x) - W_A \times [(x-3)(x-9)] \quad (56)$$

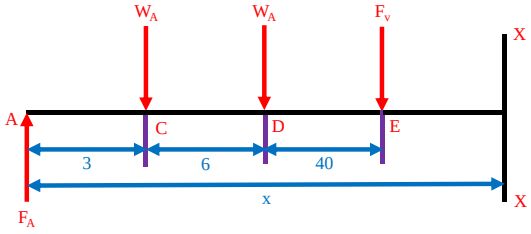

Fig. 9. Span EF (49 < x < 93).

$$SF_{XX} = F_A - 2W_A - F_v \quad (57)$$
$$BM_{XX} = F_A \times (x) - W_A \times [(x-3)(x-9)] - F_v \times (x-49) \quad (58)$$

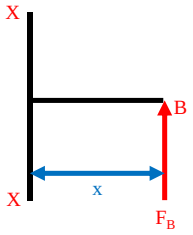

Fig. 10. Span BG (0 < x < 5).

$$SF_{XX} = -F_B \quad (59)$$

$$BM_{XX} = F_B \times (x) \quad (60)$$

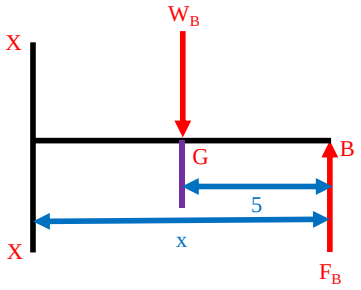

Fig. 11. Span GF (5 < x < 15).

$$SF_{XX} = -F_B + W_B \quad (61)$$

$$BM_{XX} = F_B \times (x) - W_B \times (x - 5) \quad (62)$$

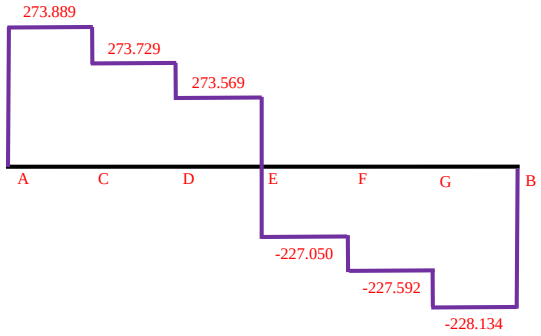

Fig. 12. Shear force diagram of worm shaft.

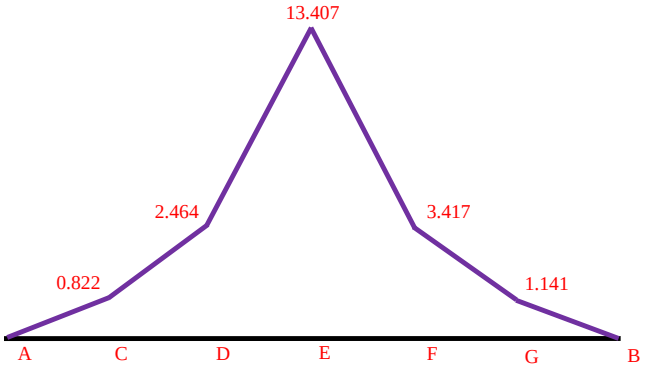

Fig. 13. Bending moment diagram of worm shaft.

Table 10. Result data for shear force and bending moment.

Parameters	Symbol	Value	Unit
Reaction force at A	F_A	273.889	N
Reaction force at B	F_B	228.134	N
Shear force at span AC	SF_{AC}	273.889	N
Shear force at span CD	SF_{CD}	273.729	N
Shear force at span DE	SF_{DE}	273.569	N
Shear force at span EF	SF_{EF}	-227.050	N
Shear force at span GF	SF_{GF}	-227.592	N
Shear force at span BG	SF_{BG}	-228.134	N
Bending moment at A	BM_A	0	Nm
Bending moment at C	BM_C	0.822	Nm
Bending moment at D	BM_D	2.464	Nm
Bending moment at E	BM_E	13.407	Nm
Bending moment at F	BM_F	3.417	Nm
Bending moment at G	BM_G	1.141	Nm
Bending moment at B	BM_B	0	Nm

3. Bending Stress Analysis of Worm and Worm Gear

The bending stress of worm and worm gear is calculated by using the following Lewis's bending stress Eq. (63) and Eq. (64)

$$\sigma_x = \frac{F_{tg}}{bm_a Y} \quad (63)$$

$$\sigma_y = \frac{F_{tw}}{bm_a Y} \quad (64)$$

Lewis form factor,

$$Y = 0.316 \quad (65)$$

Shear stress,

$$\tau_{xy} = \frac{16T_g}{\pi D_g^3} + \frac{16T_w}{\pi D_w^3} \quad (66)$$

The bending stress analysis of worm and worm gear is carried out by varying three different materials. The analysis is conducted to verify the best material for the worm and worm gear in the gear box at higher speed by analyzing stress and strain. The various mechanical properties of the selected materials are given in Table 11.

Table 11. Mechanical properties of three different materials.

Mechanical Properties	Phosphor Bronze	Aluminum Bronze	Tin Bronze
Dnesity, ρ (kg/m^3)	8800	7450	8690
Modulus of elasticity, E (GPa)	110	107	103
Poisson ratio, ν	0.341	0.3	0.28
Yield strength, σ_y (MPa)	450	221	172
Ultimate strength, σ_u (MPa)	550	568	241

Principal stresses,

$$\sigma_{1,2} = \frac{1}{2}(\sigma_x + \sigma_y) \pm \frac{1}{2}\sqrt{(\sigma_x - \sigma_y)^2 + 4\tau_{xy}^2} \quad (67)$$

By using von-Mises criteria,

$$\bar{\sigma} = \frac{1}{\sqrt{2}}\sqrt{(\sigma_1 - \sigma_2)^2 + (\sigma_2 - \sigma_3)^2 + (\sigma_3 - \sigma_1)^2} \quad (68)$$

Principal strain,

$$\varepsilon_1 = \frac{1}{E}[\sigma_1 - \nu(\sigma_2 + \sigma_3)] \quad (69)$$

$$\varepsilon_2 = \frac{1}{E}[\sigma_2 - \nu(\sigma_1 + \sigma_3)] \quad (70)$$

$$\varepsilon_3 = \frac{1}{E}[\sigma_3 - \nu(\sigma_1 + \sigma_2)] \quad (71)$$

Effective strain,

$$\bar{\varepsilon} = \left[\frac{2}{3}(\varepsilon_1^2 + \varepsilon_2^2 + \varepsilon_3^2)\right]^{1/2} \quad (72)$$

4. Numerical Analysis of Worm and Worm Gear

The model worm and worm gear is drawn by AutoCAD 2019 software as shown in Fig. 14. In this paper, the bending stress of worm and worm gear is calculated by using ANSYS 16.2 software [19, 20]. For this reason, the model of worm and worm gear in AutoCAD 2019 software is exported to ANSYS 16.2 software as an SAT file [21, 22].

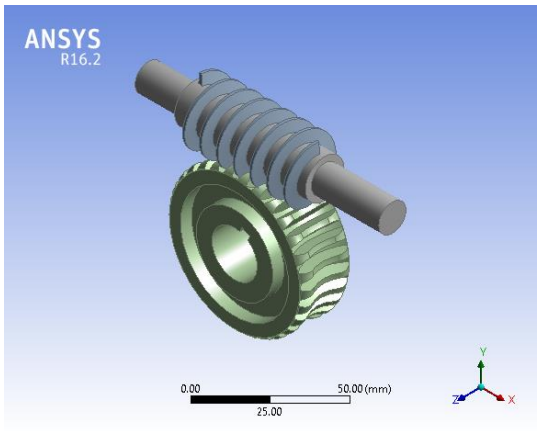

Fig. 14. Model of worm and worm gear.

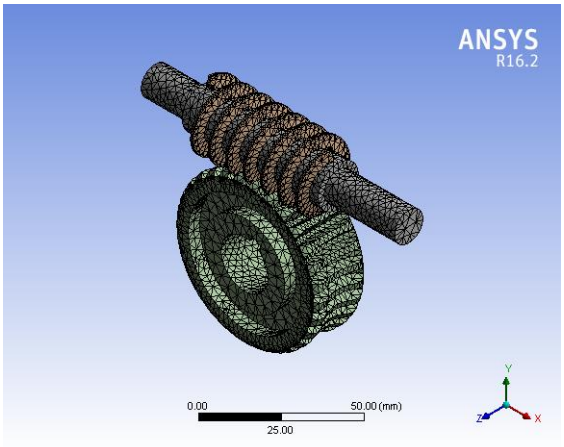

Fig. 15. Meshing of worm and worm gear.

The worm and worm gear geometry model is meshed as shown in Fig. 15. This mesh model is imported to static structural analysis [23, 24].

After applying mesh in worm and worm gear, constrain and loading condition are applied as shown in Fig. 16. The fixed support was applied to the inner rim of the worm gear and the torsional moment of 56.007 Nmm is applied to the outer rim of the worm gear. The frictionless support was applied to the shaft of the worm and the torsional moment of 2.967 Nmm is applied to the worm. And the applied tangential load of 1931.276 N is applied to the root of gear teeth and 269.727 N is applied to the tip of worm thread. Boundary condition of worm and worm gear is shown in Fig. 16.

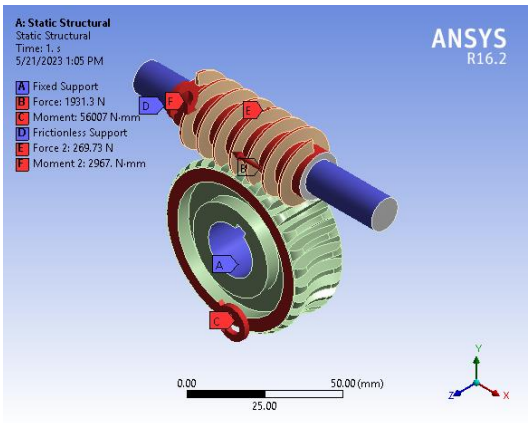

Fig. 16. Boundary conditions of worm and worm gear.

After meshing and setting up of boundary conditions of worm and worm gear, solved the solution and get equivalent von-Mises stress and effective strain of worm and worm gear. Figure 17 shows the von-Mises stress at the contact area between worm and worm gear at 122.07 MPa. Figure 18 shows the maximum effective strain of worm and worm gear and the value is 0.0012679. And the maximum von-Mises stress and effective strain of worm and worm gear developed by ANSYS 16.2 software are compared with theoretical results.

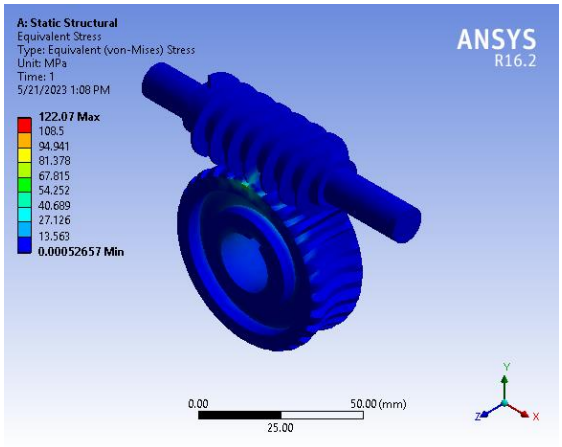

Fig. 17. Von-Mises stress of worm and worm gear (phosphor bronze).

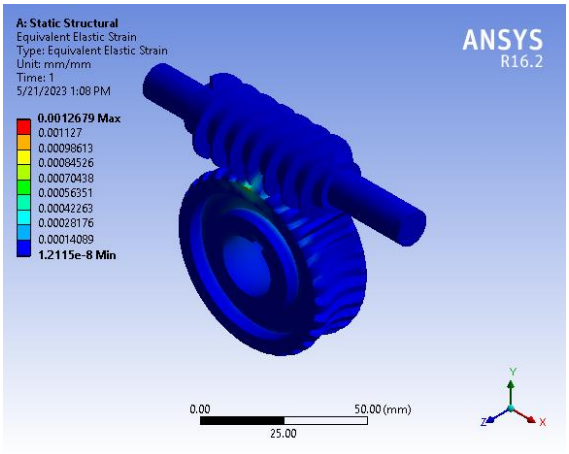

Fig. 18. Effective strain of worm and worm gear (phosphor bronze).

The bending stress of worm and worm gear is analyzed by varying three different materials and other parameters are kept constant. Figure 19 shows the simulation result of von-Mises stress for aluminum bronze worm and worm gear. The simulation result of effective strain of worm and worm gear for aluminum bronze is shown in Fig. 20.

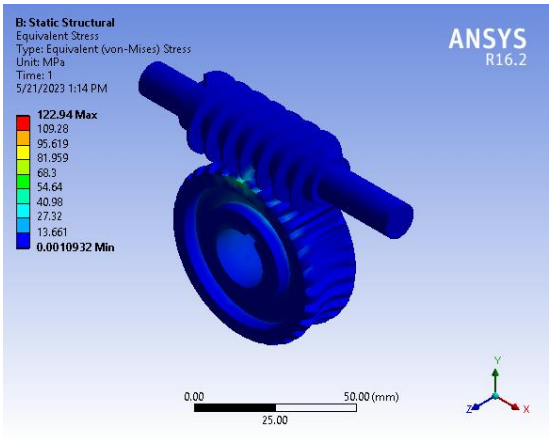

Fig. 19. Von-Mises stress of worm and worm gear (aluminum bronze).

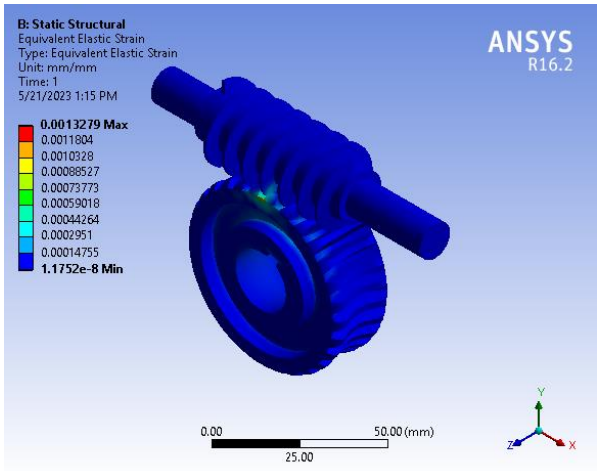

Fig. 20. Effective strain of worm and worm gear (aluminum bronze).

The simulation result of von-Mises stress for tin bronze is expressed in Fig. 21. The numerical result of effective strain of tin bronze worm and worm gear is shown in Fig. 22.

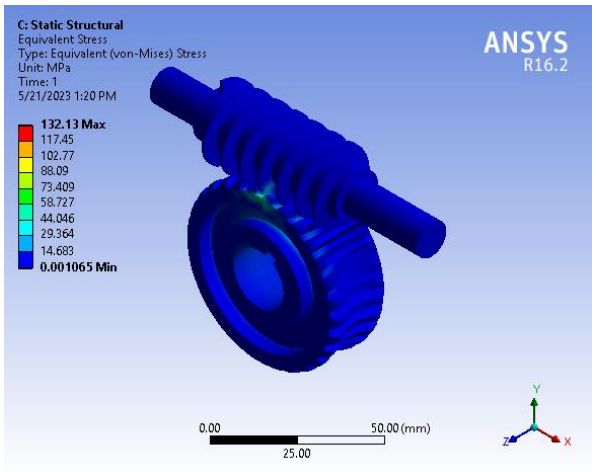

Fig. 21. Von-Mises stress of worm and worm gear (tin bronze).

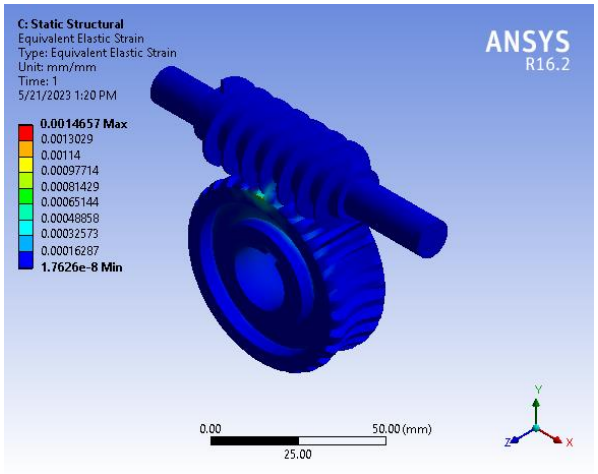

Fig. 22. Effective strain of worm and worm gear (tin bronze).

5. Result and Discussion

The comparison of von-Mises stress and effective strain of worm and worm gear from theoretical calculations and simulation results are shown in Table 12. In the following Table 12, the comparison between the theoretical and simulation results are nearly the same. So, the design is satisfying.

Table 12. Comparison of von-Mises stress and effective strain for worm and worm gear from theoretical and simulation result.

Parameters	Theoretical Result	Numerical Result	Percent Deviation
Von-Mises stress (MPa)	133.698	122.070	9%
Effective strain ($\times 10^{-3}$)	1.109	1.268	13%

The comparison of von-Mises stress values of worm and worm gear with three different materials is expressed in Fig. 23. Figure 24. shows the comparison of effective strain of worm and worm gear with three different materials.

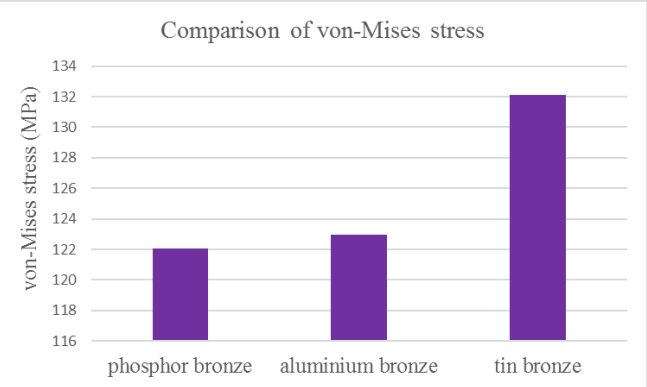

Fig. 23. Comparison of von-Mises stress with three different materials.

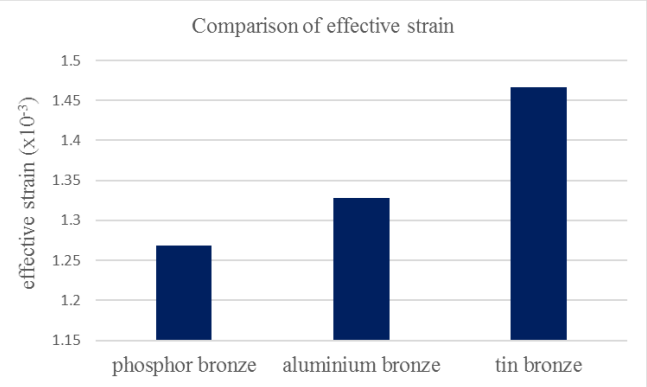

Fig. 24. Comparison of effective strain with three different materials.

From the above Fig. 23. and Fig. 24., it was found that the maximum von-Mises stress and effective strain of phosphor bronze are less than other two materials. So, the suitable material for worm and worm gear is phosphor bronze.

6. Conclusion

The design of worm and worm gear are designed for transmission system of mini power weeder. For strength check of worm and worm gear, the actual transmitted load is determined from transmitted torque. The tooth load is less than permissible tooth load. Therefore, strength check is satisfying. All gear teeth of transmission gear have sufficient strength and they are not failure under static loading and dynamics loading. So, the static tooth load and wear load are greater than dynamics tooth load. So, dynamics check is satisfactory.

In structural analysis of worm and worm gear, the structural behaviors are calculated by theoretically and numerically. The numerical von-Mises stress and effective strain of worm and worm gear are done with three different materials and are chosen the suitable material. The von-Mises stress of phosphor bronze, aluminum bronze, and tin bronze are 122.07, 122.94, and 132.13 MPa. The effective strain of three materials are 0.0012679, 0.0013279, and 0.0014657. So, phosphor bronze is suitable for worm and worm gear.

Acknowledgement

The author would like to thank to Farm Machinery Factory, Mandalay Industrial Zone for their help with permission to be able to collect the required data for mini power weeder worm and worm gear and Head of Department and all teachers from Mechanical Engineering Department for their kind supervision, encouragement, suggestion, and valuable guidelines for this paper.

References

[1] D. G. Lee, "A study on optimum design of worm ger reducer output pinion," *Journal of the Korean Society of Manufacturing Process Engineers*, vol. 16, no. 6, November 2017, doi: 10.14775/ksmpe.2017.16.6.153.

[2] A. M. Singh, M. Bhawsar, and N. K. Nagayach, "Structure analysis, contact stress analysis and fatigue life analysis of spur gear assembly by using fem," *IJO-SCIENCE*, vol. 4, no. 4, April 2018, doi: 10.24113/ijoscience.v4i4.133.

[3] C.-I. Boantă, "The comparative study on the behavior of the speed reducer with worm face gear with modified geometry," in *9th International Conference Interdisciplinarity in Engineering*, Tirgu-Mures, Romania, 2015, pp. 68-73.

[4] M. Bharati, "A performance prediction of worm-worm wheel and its multi objective design parameter optimization based on genetic algorithm," *International Journal of Scientific and Research Publication*, vol. 5, no. 2, February 2015.

[5] Y. K. Mogal, "A multi-objective optimization approach for design of worm and worm wheel based on genetic algorithm," *Bonfring International Journal of*

Man Machine Interface, vol. 3, no. 1, March 2013, doi: 10.9756/bijmmi.4403.

[6] R. O. Chime, "Design, modeling, simulation of worm gears: Analysis of worm gears," *International Journal of Engineering Science and Innovative Technology*, vol. 5, no. 5, September 2016.

[7] M. P. Thu, "Stress analysis on spur gears using ANSYS Workbench 16.0," *International Journal of Science and Engineering Applications*, vol. 7, no. 8, 2018, doi: 10.7753/ijsea0708.1016.

[8] D. Pharkute, "Case study on design and analysis of worm gear box for elevator," *International Journal of Engineering and Technology*, vol. 8, no. 5, pp. 3631-3639, May 2021.

[9] R. S. Khurmi and J. K. Gupta, "Worm gears," in *A Textbook of Machine Design*, 4th ed. New Delhi, India: Eurasia Publishing House, 2005, ch. 31, pp. 1101-1124.

[10] R. G. Budynas and J. Keith Nisbett, "Bevel and worm gears," in *Mechanical Engineering Design*, 10th ed. New York, USA: McGraw-Hill Education, 2015, ch. 15, sec. 3, pp. 777-816.

[11] S. Jyothirmai, "A finite element approach to bending, contact and fatigue stress distribution in helical gear systems," *Procedia Materials Science*, vol. 6, pp. 907-918, 2014, doi: 10.1016/j.mspro.2014.07.159.

[12] J. Venkatesh, "Design and structural analysis of high speed helical gear using ANSYS," *Journal of Engineering Research and Applications*, vol. 4, no. 3, March 2014.

[13] J. K. Mohammed, "Contact stress analysis of spur gear under the different rotational speed by theoretical and finite element method," *Academic Journal of Nawroz Univisity*, vol. 7, no. 4, 2018, doi: 10.25007/ajnu.v7n4a292.

[14] Kolase Sachin A. and Randhavan B. M., "Experimental stress analysis of worm gear using 3D photo elasticity and its validation through finite element analysis," *International Journal of Advance Research, Ideas and Innovations in Technology*, vol. 7, no. 4, pp. 1656-1660, 2021.

[15] F. Yang, "Finite element modelling and load shear analysis for involute worm gears with localized tooth contact," in *Proc. Instn. Mech Engrs.*, 2001, vol. 215, doi: 10.1115/detc2000/ptg-14402.

[16] D. Miltenovic, "Load capacity of worm gears with compact design," *Annals of Faculty Engineering Hunedoara - International Journal of Engineering*, vol. 14, no. 1, February 2016.

[17] P. Chotickai, "Stress analysis of rib-to-deck joints in orthotropic steel deck based on nominal and effective notch stress approaches," *Engineering Journal*, vol. 25, no. 7, pp. 17-30, July 2021, doi: 10.4186/ej.2021.25.7.17.

[18] S. Tirapat, "Influence of surface stresses on the deflection of circular nanoplate with two-parameter elastic substrate," *Engineering Journal*, vol. 26, no. 10, pp. 99-110, October 2022, doi: 10.4186/ej.2022.26.10.99.

[19] F. L. Litvin and A. Nava, "New geometry of worm face gear drives with conical and cylindrical worms: Generation, simulation of meshing, and stress analysis," National Aeronautics and Space Administration, Glenn Research Center, University of Illinois at Chicago, Chicago, Illinois, 2002.

[20] A. H. Falah, "Load and stress analysis of cylindrical worm gear using tooth slicing method," *Transactions of the CSME/de la SCGM*, vol. 30, no. 1, October 2005, doi: tcsme-2006-0007.

[21] D. Su, "Optimum design of worm gears with multiple computer aided techniques," in *Proceedings of ICCES'08*, 2008, pp. 575-581.

[22] D. Jeeva, "Analysis on bending stress of helical gear," *Natural Volatiles and Essential Oils*, vol. 8, no. 5, pp. 3384-3393, 2021.

[23] R. Mailapalli, "Design and assembly analysis of a worm-assembly in a gear box," *International Journal and Magazine of Engineering, Technology, Management and Research*, vol. 4, no. 4, pp. 86-96, April 2017.

[24] V. Patel, "Contact stresses and dynamic analysis of involute spur gear with FEM approach," *International Journal for Research in Applied Science and Engineering Technology*, vol. 9, no. 10, October 2021, doi: 10.22214/ijraset.2021.38600.

Zaw Htet Win was born in Mandalay, Myanmar in 1991. He received BE (Mechanical Engineering) degree from the Technological University (Mandalay), Myanmar in 2013 and ME (Mechanical Engineering) degree from the Mandalay Technological University, Myanmar in 2016.

From 2017 to 2021, he was a Demonstrator with the Mechanical Engineering Department, Mandalay Technological University. Since 2021, he has been an Assistant Lecturer with the Mechanical Engineering Department, Mandalay Technological University. His research interests include agricultural machine design and performance.

Mr. Zaw Htet Win was a recipient of the International Institute of Engineers and Researchers Excellent Paper Award in October, 2023.

War War Min Swe was born in Chauk, Magway, Myanmar in 1974. She received BE (Mechanical Engineering) degree from the Mandalay Technological University, Myanmar in 2002 and also ME (Mechanical Engineering) degree from the Institute Teknologi Bandung (ITB), Indonesia in 2005 and Ph.D. (Mechanical Engineering) from the Nagasaki University, Japan in 2017.

From 2018 to 2021, she was an Associate Professor with the Mechanical Engineering Department, Mandalay Technological University. Since 2021, she has been a Head and Professor with the Mechanical Engineering Department, Mandalay Technological University. She is the author of 5 articles. Her research interests include turbomachinary and fluid mechanism.

Dr. War War Min Swe was a speaker of the AUN/SEED-Net FIELD-WISE SEMINAR on Mechanical and Aeronautical Engineering in Indonesia, 2004.

Aung Ko Latt was born in Magway, Myanmar in 1980. He received BE (Mechanical Engineering) degree from the Mandalay Technological University, Myanmar in 2003 and also ME (Mechanical Engineering) degree in 2009 and Ph.D. (Mechanical Engineering) degree in 2017. He also received MBA degree from Meiktila University of Economics, Myanmar in 2021.

From 2017 to 2021, he was an Associate Professor with the Mechanical Engineering Department, Mandalay Technological University. Since 2021, he has been a Professor with the Mechanical Engineering Department, Mandalay Technological University. His research interests include machine design, heat transfer, and thermodynamics section.

Dr. Aung Ko Latt was a speaker of the International Conference on Mechanical, Aeronautics and Production Engineering (ICMAPE) in Thailand, 2015.